

Study of Impact Ionization Coefficients in Silicon With Low Gain Avalanche Diodes

Esteban Currás Rivera¹ and Michael Moll¹

Abstract—Impact ionization in silicon devices has been extensively studied and several models for a quantitative description of the impact ionization coefficients have been proposed. We evaluate those models against gain measurements on low-gain avalanche diodes (LGADs) and derive new parameterizations for the impact ionization coefficients optimized to describe a large set of experimental data. We present pulsed infrared (IR)-laser-based gain measurements on five different types of 50 μm -thick LGADs from two different producers centro nacional de microelectrónica (CNM) and Hamamatsu Photonics (HPK) performed in a temperature range from $-15\text{ }^\circ\text{C}$ to $40\text{ }^\circ\text{C}$. Detailed technology computer-aided design (TCAD) device models are conceived based on secondary ion mass spectrometry (SIMS) doping profile measurements and tuning of the device models to measure C - V characteristics. Electric field profiles are extracted from the TCAD simulations and used as input to an optimization procedure (least squares fit) of the impact ionization model parameters to the experimental data. It is demonstrated that the new parameterizations give a good agreement between all measured data and TCAD simulations which is not achieved with the existing models. Finally, we provide an error analysis and compare the obtained values for the electron and hole impact ionization coefficients against existing models.

Index Terms—Avalanche breakdown, electron multiplication, gain, hole multiplication, impact ionization, low gain avalanche diode (LGAD).

I. INTRODUCTION

IMPACT ionization in silicon arising from dedicated high-field regions in devices, has been deeply studied and exploited for several sensor types over many decades. More recently, low-gain avalanche diodes (LGADs) were developed within the RD50 collaboration to gain an internal signal amplification device for particle detection [1]. They are implemented as n^{++} - p^+ - p avalanche diodes, where the highly-doped p^+ layer is added to create a very high electric field region. This electric field generates the avalanche multiplication of the primary electrons coming from the bulk of the device, creating additional electron-hole pairs in the gain layer (GL)

Manuscript received 20 December 2022; revised 10 March 2023; accepted 4 April 2023. Date of publication 3 May 2023; date of current version 25 May 2023. The review of this article was arranged by Editor J. Mateos. (Corresponding authors: Esteban Currás Rivera; Michael Moll.)

The authors are with the Experimental Physics Department, CERN (Organization Européenne Pour la Recherche Nucléaire), 1211 Geneva, Switzerland (e-mail: ecurrasr@cern.ch; michael.moll@cern.ch).

Color versions of one or more figures in this article are available at <https://doi.org/10.1109/TED.2023.3267058>.

Digital Object Identifier 10.1109/TED.2023.3267058

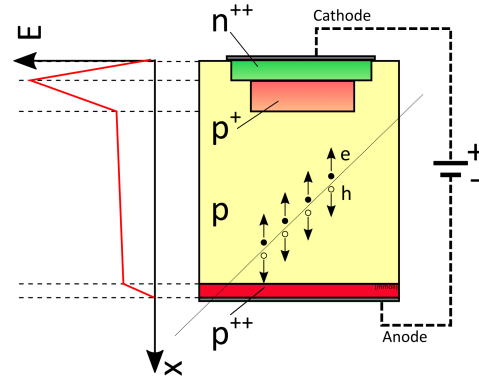


Fig. 1. Sketch of the cross section of a pad-like LGAD with a charged particle passing through. The very highly doped implants of the front (n^{++}) and the back (p^{++}) electrode as well as the GL implant (p^+) within the high resistivity bulk (p) are shown. A qualitative profile of the electric field strength $E(x)$ is depicted too, where the peak is located in the GL region. Electrons entering the high field region are leading via impact ionization to an avalanche process. The resulting electrons are collected at the front electrode while the resulting holes drift to the back electrode generating the amplified signal.

region. A schematic cross section of a standard pad-like LGAD is shown in Fig. 1. The LGAD structure is designed to exhibit a moderate gain over a wide range of reverse bias voltage until the avalanche breakdown takes place. The LGAD technology is of high interest in the field of high energy physics (HEPs) as a 4-D tracking device [2]. It has been qualified for use in the minimum ionizing particle (MIP) timing detector of the CMS experiment and the high-granularity timing detector (HGTD) of the ATLAS experiment for the high luminosity large hadron collider (HL-LHC) operations [3], [4].

To maximize the performance of LGADs, the device parameters have to be very carefully tuned to achieve the anticipated gain under the defined operational conditions [1], [5]. This requires reliable and precise impact ionization models to predict the gain in the design phase of the devices. There are several studies and impact ionization models proposed in [6], [7], [8], [9], and [10]. However, recent works on technology computer-aided design (TCAD) simulations of the gain of LGAD sensors have shown that the various impact ionization models deliver on the one hand significantly different results, and on the other hand exhibit often a limited agreement between simulated and experimental data [11], [12], [13].

This is partly due to the challenge to implement very precise device models that yield accurate electrical field configurations for the simulation. Especially the profiles of the implants that

shape the high electric field region are not well known and can deviate between the anticipated (i.e., simulated profile) and the profile obtained during the fabrication process. The exponential dependence of the impact ionization coefficients on the electric field strength, and the exponential dependence of the multiplication factors on the length of the high electric field regions, result in big variations of the obtained gain with small changes in those device parameters.

Another source of uncertainty is coming from the measurements used to characterize the impact ionization. The measured gain is very sensitive to temperature and applied voltage calling for precise measurements of these parameters. More importantly, the measured gain can be reduced when high charge densities undergo amplification and create sufficiently high space charge densities to significantly reduce the electric field strength [14]. If not taken into account in both, measurement and modeling, this easily leads to errors in the impact ionization modeling.

All the above-mentioned factors have to be carefully taken into account to properly model impact ionization in LGADs and are addressed in this article. In the following, we describe the used samples and the employed measurement and simulation techniques (Section II), followed by a detailed explanation of the methodology used to obtain a new set of parameters for the investigated impact ionization coefficients models (Section III). Finally, we present the experimental data and the new optimized parameter sets with an in-depth error discussion (Section IV) and summarize our findings (Section V).

II. DESCRIPTION AND CHARACTERIZATION OF THE SAMPLES

The samples used for this study were LGAD and p-i-n sensors produced by Hamamatsu Photonics (HPK) and centro nacional de microelectrónica (CNM)-IMB. The LGAD and p-i-n sensors from the respective producers differed only in the addition of the p⁺-implant, i.e., the GL, for LGADs. The HPK samples were from the production run S10938-6130 (also called HPK prototype 2 or HPK2) produced on a wafer with a 50 μm epitaxial layer on a 150 μm thick low resistivity support wafer. The CNM samples were from the production run 12916, produced on a 50 μm Float Zone wafer bonded to a 300 μm low resistivity Czochralski wafer as support. The CNM LGADs were designed with a shallow GL doping profile and the same doping concentration for all devices investigated in the present work. The HPK ones have a deep GL doping profile and were produced in four different splits (S1–S4) that differed in the doping concentration of the GL and consequently in the gain. The secondary-ion mass spectrometry (SIMS) profiles visualize the difference between shallow and deep GLs and are explained in more detail in Section II-B.

All samples have an active area of 1.3 × 1.3 mm² and a guard ring structure surrounding the central pad. To allow laser illumination from the pad side (i.e., the front electrode), they have an opening window of 100 × 100 μm² in the metallization. In Fig. 2, two pictures of sensors studied in this work are shown, and in Table I the key parameters of the samples are listed. The full depletion voltage (V_{dep}), the

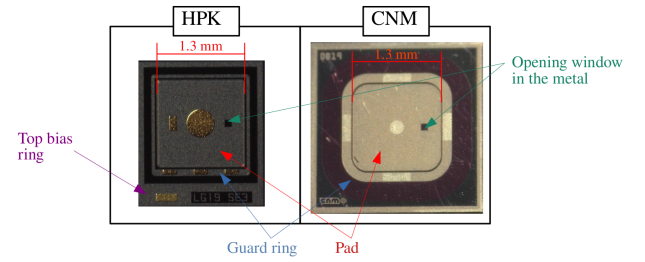


Fig. 2. Photographs (not scaled) of the two LGAD types studied in this work. The left picture shows a top view of an LGAD produced by HPK and the right one the top view of an LGAD produced by CNM. The corresponding p-i-n sensors of the two producers look identical.

TABLE I

MAIN PARAMETERS FOR THE LGAD SAMPLES USED IN THIS WORK. THE FULL DEPLETION VOLTAGE (V_{dep}), THE GL DEPLETION VOLTAGE (V_{gl}), THE AVERAGE BREAKDOWN VOLTAGE (V_{bd}) AT 20 °C, THE CAPACITANCE REACHED ABOVE FULL DEPLETION (C_{end}) AND THE ACTIVE THICKNESS (d) ARE GIVEN

Sample	V_{dep} [V]	V_{gl} [V]	$V_{bd}(20^{\circ}\text{C})$ [V]	C_{end} [pF]	d [μm]
HPK-S1	61.7	54.5	145	3.6	48
HPK-S2	59.7	53.5	168	3.6	48
HPK-S3	58.4	51.2	212	3.6	48
HPK-S4	57.9	50.7	235	3.6	48
CNM	42.8	39.4	112	4.2	42

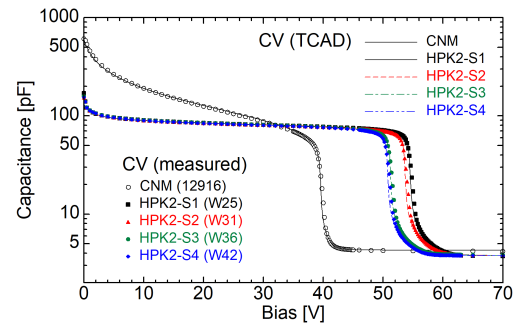


Fig. 3. Capacitance versus voltage measurements (symbols) and corresponding TCAD simulations (lines) of the five LGAD types used for this work. The C–V curves were obtained at 20 °C with a measurement frequency of 1 kHz.

depletion voltage of the GL of the LGAD (V_{gl}), the breakdown voltage at 20 °C [$V_{bd}(20^{\circ}\text{C})$], the end capacitance of the LGAD sensors reached upon full depletion of the device (C_{end}) and the active thickness of the sensors (d) are given.

A. Electrical Characterization

The electrical characterization was performed at the solid state detectors (SSD) laboratory at CERN. A probe station was used to measure the leakage current and the capacitance as a function of the reverse bias voltage (I – V and C – V). The bare samples were placed directly on a temperature-controlled chuck. During the electrical characterization the guard ring was connected to the ground. All measurements were performed at 20 °C and the frequency in the LCR meter sinusoidal signal was set to 1 kHz with an amplitude of 0.5 V. More details about the setup can be found in [15]. In Fig. 3, the C–V curves for the different LGAD types used in this work are shown.

The GL doping profiles $N_x(x)$ as function of depth (x) were extracted from the C–V curves using in the following

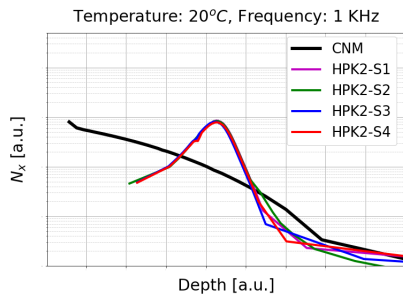


Fig. 4. GL doping profiles extracted from the C - V measurements shown in Fig. 3 by employing (1).

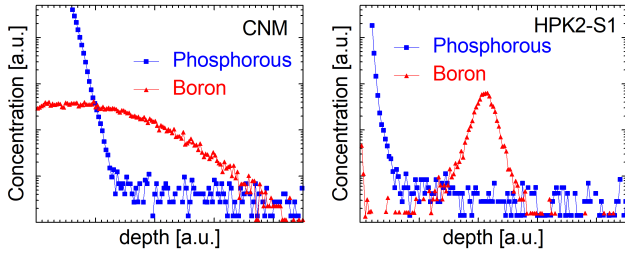


Fig. 5. Phosphorous and boron concentration profiles as measured with SIMS in the GL region of the CNM LGAD type (left) and the HPK2 S1 LGAD type (right).

equation [16]:

$$N_x(x) = \frac{C^3}{q\epsilon_0\epsilon_r A^2 dc/dV} \quad \text{with} \quad x = \frac{\epsilon_0\epsilon_r A}{C} \quad (1)$$

where C is the capacitance and A the area of the sensor, q the elementary charge, ϵ_0 the permittivity of vacuum and ϵ_r the relative permittivity of silicon. The extracted doping profiles are given in Fig. 4. We can clearly distinguish the two different doping profiles used by the two producers: shallow by CNM and deep by HPK. It is however noted that the doping profile is extracted under the assumption of a constant area A in (1). This assumption is a good estimate for the p-i-n diodes but is only approximate for the small LGAD sensors with a wide junction termination extension (JTE) as in the present case. The presence of the JTE and the lateral extension of the electric field, with growing bias voltage, allow only an approximate estimation of the doping profile employing (1). This is the reason why SIMS measurements (see Section II-B), in combination with TCAD modeling (see Section III-B), were employed to extract the doping profiles and finally the electric field profiles.

B. SIMS Measurements

SIMS analyses were performed on two types of samples at the SGS Institute Fresenius GmbH in Dresden, Germany. One CNM LGAD and one HPK2 S1 type LGAD were selected. The analysis of the data allowed us to extract the phosphorous and boron concentrations in the GL region up to several microns in depth. In Fig. 5, the results of the measurements for the two sample types are shown in arbitrary units, with a linear x -axis and a logarithmic y -axis. In both cases, the boron concentration measured with SIMS, reflects the shape of the active boron profiles shown in Fig. 4 and extracted from the C - V measurements given in Fig. 3. Absolute values

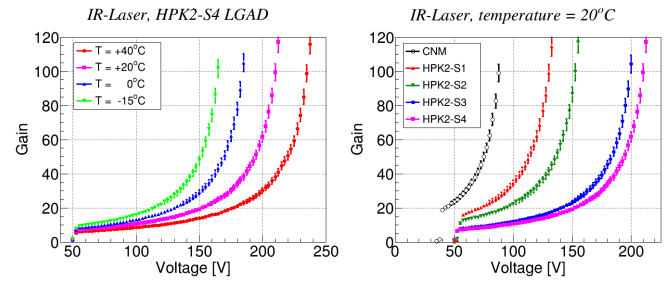


Fig. 6. On the left side: gain measured with the IR-laser at different temperatures for the HPK2-S4 LGAD. On the right side: gain measured at 20 °C for all the LGAD types. The experimental error in the measurements is $\sim 5\%$.

are not shown as requested by non-disclosure agreements with the sensor suppliers.

C. Gain Measurements With IR-Laser

The gain of the LGADs was measured using a pulsed infrared (IR)-laser with a wavelength of 1060 nm in the transient current technique (TCT) setup of the SSD group at CERN. The IR-laser intensity was tuned to generate an equivalent charge of ~ 1 MIP in the detectors and the spot size was $\varnothing \approx 80 \mu\text{m}$. These two values were chosen to have a good SNR with low charge density inside the detector bulk to avoid any gain reduction up to a gain of 100. The gain was evaluated as the ratio between the charge measured in the LGAD and the charge measured in the p-i-n (after full depletion), both measured under the same conditions. The MIP equivalent charge calibration of the setup was determined by using a ^{90}Sr beta source on the same sensors. More details about the used TCT setup and the method employed to measure the gain with an IR-laser can be found in [14].

The gain was measured at four different temperatures: -15°C , 0°C , 20°C , and 40°C . Several samples were measured to estimate the error in the gain measurements, which was found to be in the order of 5%. This includes systematic errors in the measurements, fluctuation in the laser intensity, fluctuations in the temperature during measurements, and variation in the gain between “identical” LGADs (with the same expected gain by design). In Fig. 6, the gain at different temperatures for the HPK2 S4 LGAD is shown on the left side, and the gain measured at 20 °C for all used LGAD types on the right side.

III. METHODOLOGY USED FOR EXTRACTING IMPACT IONIZATION PARAMETERS

TCAD device simulations were performed in order to determine the electric field profiles as a function of bias voltage in all LGAD sensors using the Sentaurus Device software from Synopsys [17]. In the following, we describe the implementation of the sensor geometry in TCAD and the tuning of geometrical parameters by employing C - V measurements and other characterization techniques on the used devices (see Section III-A). Once the sensor geometry was optimized, the electric field strength maps were calculated as a function of voltage and, the gain of the LGADs was simulated with Sentaurus TCAD using the various impact ionization models available within the tool, as well as the

model described by Massey et al. [7] (see Section III-B). This procedure is very similar to the works presented in [11], [12], and [13] and as it was observed in these previous works, we could not find a model that gives a fully satisfying match to our experimental data. In consequence, we started a model parameter optimization procedure for the three most commonly used models which we label in the following as Massey et al. [7], Overstraeten and Man [8], and Okuto and Crowell [9]. For the optimization process, the electric field strength maps as a function of voltage were extracted from TCAD and used as input in a custom-written C++ code for parameter optimization. The TCAD simulations and the C++ code delivered the same LGAD gain values for identical input parameters, with however the C++ code being much faster and therefore convenient for parameter fitting. The so-called gain reduction mechanism [14] was carefully avoided in both, the experimental work and the TCAD simulations. The overall procedure is described in the following in more detail.

A. Implementation of LGAD Device Models in TCAD

The LGAD and p-i-n geometries were implemented in Synopsys TCAD including the JTE and guard ring structures. For the CNM samples, the producer provided a complete mask set for all process steps and information on the process parameters used for the various implantation and high-temperature steps. For the HPK samples only the metal mask layer was available. As for all used device types no sensors with different sizes, i.e., a different ratio of central pad size to periphery length, were available, it was not possible to correct experimentally for periphery effects by subtracting the $C-V$ curves obtained from different size samples. Therefore, the sensor periphery was implemented in the TCAD simulations to obtain the simulated $C-V$ of the full devices. For all sensor types high resolution optical images were produced to verify metal dimensions and provide input on other structures that were optically visible through their requirement of being based on an etching process. The active sensor thickness as well as the bulk doping concentration was extracted from $C-V$ measurements of the p-i-n and LGAD sensors. Finally, the doping profiles of the front phosphorus implant and the GL boron profile for the CNM LGAD and the HPK2 S1 LGAD were extracted from the SIMS measurements presented in Section II-B and fed into the TCAD simulations. The measured depletion voltage of the GL (V_{gl}) was then used to fine-tune the doping concentration of the GL in the TCAD simulations. A reduction of the GL boron profile as measured by SIMS by 8% for the HPK2 S1 LGADs and by 5% for the CNM LGADs resulted in a perfect agreement of the V_{gl} in simulation and measurements. The difference between the GL boron concentration as measured by SIMS against the active boron concentration used in the TCAD simulation of a few percent could be attributed to the fact that SIMS measures the total atomic boron concentration while for the electrical device properties only the electrically active boron is relevant, and only part of the implanted boron is activated. On the other hand, the difference might also only reflect the measurement error of the SIMS method itself.

For the HPK2 LGADs of splits 2-4, no SIMS measurements were available and the GL doping profile was assumed to have

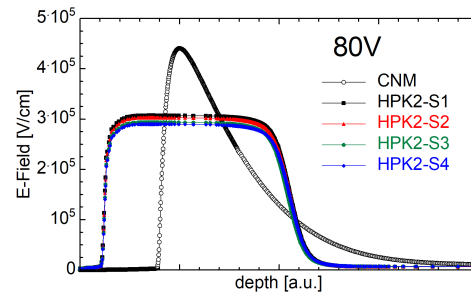


Fig. 7. Simulated electric field strength profiles $E(x)$ at the same bias voltage (80 V) for the five studied LGAD types.

the same shape as the one of split 1. This is a very reasonable assumption taking the doping profiles extracted from $C-V$ measurements shown in Fig. 4. The peak of the doping profile was found to be at the same position for splits 1-4, while it was slightly shifted to the surface for split 3. The concentration for all splits was adapted to match the measured V_{gl} . The good agreement between the measured $C-V$ curves and the $C-V$ curves simulated in TCAD, can be seen Fig. 3 where both, measured and simulated data, are displayed.

B. TCAD Simulations of Electric Field Profiles and Gain Curves

The TCAD model described in the previous section resulted in detailed electric field profiles. The experimental gain measurements were obtained with the TCT technique by shining the laser onto a central part of the sensor. Therefore, at the measurement position, the electric field (and the gain) is not influenced by the LGAD periphery and can be simulated with a much simpler 1-D geometry. Three-dimensional and 1-D simulations of the electric field and the gain in the measurement position showed no difference. As an example, depth profiles of the electric field strength for all five LGAD types at a voltage of 80 V are shown in Fig. 7.

The TCAD simulation of gain curves as a function of voltage and temperature followed the same procedure as the experimental work. The gain for a given voltage was obtained by dividing the simulation result for the LGAD by the result for the corresponding p-i-n sensor extracted above full depletion. The gain was determined by either simulating time-resolved TCT measurements or by simulating steady-state leakage current with a homogeneous shockley-read-hall (SRH) generation across the bulk of the device. Both methods yield the same gain values for voltages above device depletion and as long as the regime for gain reduction effects is avoided [14].

All impact ionization models available in the Sentaurus software and the Massey model were tested using the default parameter sets, i.e., the published parameter sets. Fig. 8 gives a comparison of the experimental and simulated gain curves for the Overstraeten model. For better visibility, only data at 20 °C are presented. It is clearly visible that the Overstraeten model with default parameters gives higher gain values than measured. In Fig. 9, data for the LGAD type HPK2-S3 are shown. For the data at 20 °C (Fig. 9, left) the Massey and Okuto-Crowell models underestimate the gain while the Overstraeten model overestimates the gain. This disagreement motivated us to optimize the parameters of these models to

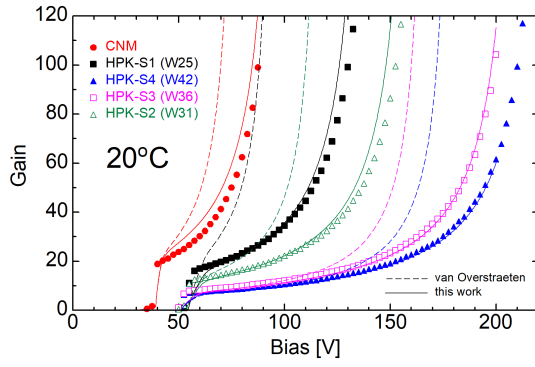


Fig. 8. Comparison between measured and simulated gain using the Overstraeten model with default parameters for all LGAD devices studied in this work (data taken at 20 °C). Measured data are given by the symbols. The TCAD simulations are shown as lines: dashed lines for the model with default parameters and solid lines for the model with optimized input parameters.

get a better agreement between measured and simulated data, as demonstrated in Fig. 9 (right) and described in more detail below. For a faster optimization of the parameters, the impact ionization equation was implemented in C++, and by the end of the process, the models with the optimized parameters were tested in TCAD (see e.g., Figs. 8 and 9). Both simulation methods, TCAD and C++, gave the same gain.

C. Optimization Procedure of Impact Ionization Parameters

The impact ionization model parameters were adjusted by a custom-written C++ program to match our experimental data. The program allowed us to calculate the LGAD gain as a function of voltage and temperature based on the input of the electric field strength profile from the TCAD simulations. The calculations are based on the solution of the differential equation for the electron (J_n) and hole (J_p) current densities under impact ionization [18]

$$\frac{dJ_p}{dx} = \frac{-dJ_n}{dx} = \alpha_n J_n + \alpha_p J_p + g(x) \quad (2)$$

with α_n and α_p being the impact ionization coefficients (in units of cm^{-1}) for electrons and holes respectively, and $g(x)$ describing the generation of excess charge carriers. The solution is given by

$$J = M_n J_n(d) + M_p J_p(0) + \int_0^d g(x) M(x) dx \quad (3)$$

with

$$M(x) = \frac{\exp\left(-\int_x^d (\alpha_n - \alpha_p) d\eta\right)}{1 - \int_x^d \alpha_n \exp\left(-\int_\xi^d (\alpha_n - \alpha_p) d\eta\right) d\xi} \quad (4)$$

and $M_n = M(x = d)$ being the multiplication of electrons injected from the back-electrode at $x = d$ and $M_p = M(x = 0)$ the multiplication of holes injected from the front-electrode at $x = 0$. As the charge in our case is generated by the laser illumination throughout the bulk, only the last term in (3) is relevant and was taken into account in the numerical calculations.

Three different models for the impact ionization coefficients $\alpha_{n,p}$ were implemented and optimized for their parameters.

These models are “local,” which means that the ionization coefficients depend only on the local electric field. They follow the Chynoweth law [19], but each uses a different formalism for the parameterization as follows.

- 1) In the **Massey model** [7] the $\alpha_{n,p}$ coefficients follow the equation

$$\alpha_{n,p}(E, T) = A_{n,p} \exp\left(-\frac{C_{n,p} + D_{n,p} \cdot T}{E}\right) \quad (5)$$

with E being the electric field strength, T the absolute temperature, and $A_{n,p}$, $C_{n,p}$ and $D_{n,p}$ the six model parameters for the two impact ionization coefficients.

- 2) In the **Overstraeten model** [8], the $\alpha_{n,p}$ are described by

$$\alpha_{n,p}(E, T) = \gamma A_{n,p} \exp\left(-\gamma \frac{B_{n,p}}{E}\right) \quad (6a)$$

$$\text{with } \gamma = \frac{\tanh\left(\frac{\hbar\omega_{\text{op}}}{2kT_0}\right)}{\tanh\left(\frac{\hbar\omega_{\text{op}}}{2kT}\right)} \quad (6b)$$

where k is the Boltzmann’s constant, $T_0 = 300$ K is the reference temperature, the parameter $\hbar\omega_{\text{op}}$ stands for the optical phonon energy and $A_{n,p}$ and $B_{n,p}$ are further parameters.

- 3) In the **Okuto-Crowell model** [9], the $\alpha_{n,p}$ coefficients follow the equation:

$$\alpha_{n,p}(E, T) = A_{n,p} (1 + (T - 300)C_{n,p}) E \times \exp\left[-\left(\frac{B_{n,p}(1 + (T - 300)D_{n,p})}{E}\right)^2\right] \quad (7a)$$

and eight parameters $A_{n,p}$, $B_{n,p}$, $C_{n,p}$, and $D_{n,p}$.

The original values (i.e., the published values and default values in Synopsys TCAD) for the different parameters in the equations above are listed in Table II for Massey, Table III for Overstraeten and Table IV for Okuto-Crowell. For the Overstraeten model, only the values for the low electric field region ($E < 4.0 \times 10^5$ V cm^{-1}) are given, as in our parameterization we used only one set of parameters and not two as in the original publication.

The optimization of the parameters was done using the least squares method and therefore the sum of the squares of the normalized residuals was minimized for each model. The residuals were defined as the difference between the measured gain and the value provided by the model, divided by the measured gain.

IV. OPTIMIZED PARAMETERS FOR IMPACT IONIZATION MODELS

The full experimental data set of gain measurements for the five LGAD types up to a gain of 100 and in the temperature range from -15 °C to 40 °C, was subjected to the optimization procedure described in Section III in a single fit for each model. The optimal values for the different parameters in the equations can be found in Tables II–IV. With the default parameterization, the result of the sum of the residuals squared

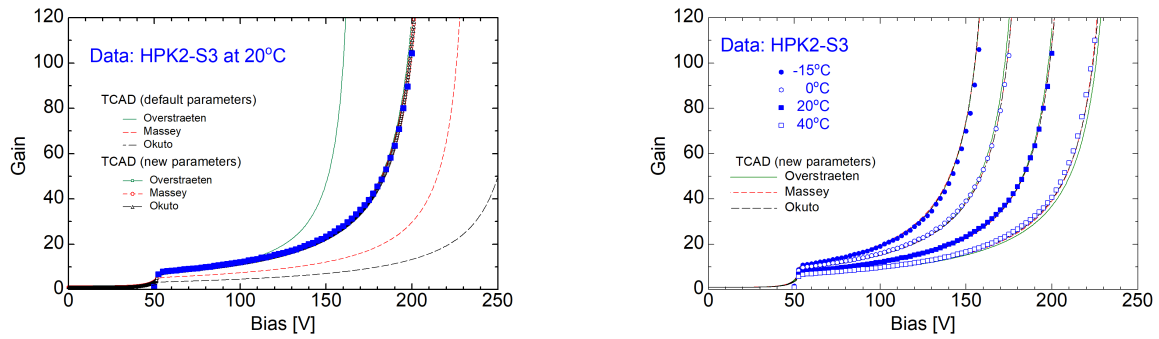


Fig. 9. (Left) Measured gain values for the HPK2-S3 device type at 20 °C (symbols), and TCAD simulations for three different impact ionization models with default parameters (lines) and optimized parameters (lines with symbols). The optimized parameters give a good agreement, while the default parameters give deviations. (Right) Simulations with optimized parameters for the three indicated models at various temperatures.

TABLE II

IONIZATION PARAMETERS FOR THE MASSEY MODEL. THE DEFAULT VALUES ARE ON THE LEFT SIDE OF THE TABLE AND THE OPTIMIZED VALUES FROM THIS ARTICLE ARE ON THE RIGHT

Parameter	Massey default		Massey optimized	
	electrons	holes	electrons	holes
$A [\times 10^5 \text{ cm}^{-1}]$	4.43	11.3	11.86	22.50
$C [\times 10^5 \text{ Vcm}^{-1}]$	9.66	17.1	10.20	18.51
$D [\times 10^2 \text{ Vcm}^{-1} \text{ K}^{-1}]$	4.99	10.9	10.43	18.28

TABLE III

IONIZATION PARAMETERS FOR THE OVERSTRAETEN MODEL. THE DEFAULT VALUES ARE ON THE LEFT SIDE OF THE TABLE AND THE OPTIMIZED VALUES FROM THIS ARTICLE ARE ON THE RIGHT.

THE PARAMETERS SHOWN IN THE TABLE CORRESPOND TO THE LOW ELECTRIC FIELD ONES: $E < 4.0 \times 10^5 \text{ V cm}^{-1}$

Parameter	Overstraeten default		Overstraeten optimized	
	electrons	holes	electrons	holes
$A [\times 10^5 \text{ cm}^{-1}]$	7.03	15.82	11.49	25.19
$B [\times 10^6 \text{ Vcm}^{-1}]$	1.231	2.036	1.325	2.428
$\hbar\omega_{op} [\times 10^{-2} \text{ eV}]$	6.3	6.3	7.58	7.58

TABLE IV

IONIZATION PARAMETERS FOR THE OKUTO-CROWELL MODEL. THE DEFAULT VALUES ARE ON THE LEFT SIDE OF THE TABLE AND THE OPTIMIZED VALUES FROM THIS ARTICLE ARE ON THE RIGHT

Parameter	Okuto-Crowell default		Okuto-Crowell optimized	
	electrons	holes	electrons	holes
$A [\text{V}^{-1}]$	0.426	0.243	0.289	0.202
$B [\times 10^5 \text{ Vcm}^{-1}]$	4.81	6.53	4.01	6.40
$C [\times 10^{-4} \text{ K}^{-1}]$	3.05	5.35	9.03	-22.0
$D [\times 10^{-4} \text{ K}^{-1}]$	6.86	5.67	11.1	8.25

was 30.4 for Massey (underestimates the gain), 5.39×10^4 for Overstraeten (overestimates the gain), and 38.3 for Okuto-Crowell (underestimates the gain). After the optimization of the parameters, the sum of the residuals was reduced to: 0.515 for Massey, 0.681 for Overstraeten, and 0.556 for Okuto-Crowell. For each model, the number of points included in the fit was 80. With all three models, the simulated gain was in good agreement with the measured gain in all the LGADs across the full experimental data range. The maximum simulated electric field was $4.5 \times 10^5 \text{ Vcm}^{-1}$ and the lowest electric field, for which we had sensitivity, was $2.8 \times 10^5 \text{ Vcm}^{-1}$. A detailed comparison between experimental data and the gain simulations using the models with the optimized parameters is given in the following.

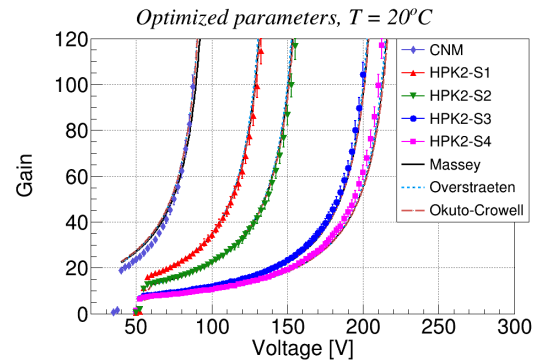


Fig. 10. Agreement between the measured and simulated gain, at 20 °C, after the optimization of the parameters for the three models.

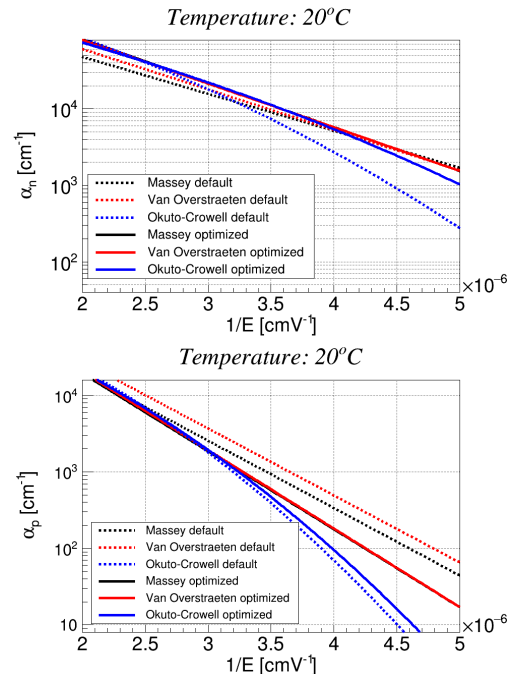


Fig. 11. Impact ionization coefficients as a function of the electric field at 20 °C. Coefficients based on the original model values (dashed lines) and the optimized parameters are shown.

A. Electric Field Dependence of Impact Ionization

The agreement between the model with the new parameterization, as obtained with the C++ code, and the measured gain at 20 °C is shown in Fig. 10. After the optimization of

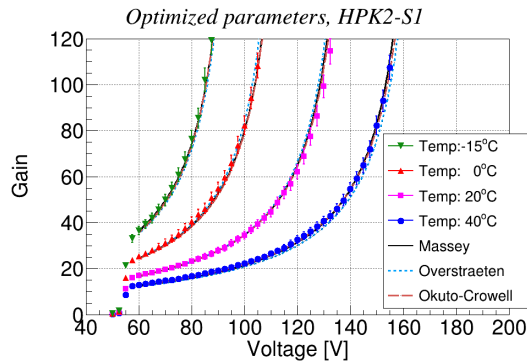


Fig. 12. Measured and simulated gain of the HPK2-S1 LGAD at different temperatures, after the optimization of the parameters for the three models.

the parameters, all three models converge to almost identical solutions. The new $\alpha_n(E)$ and $\alpha_p(E)$ coefficients as a function of the electric field at 20 °C are shown in Fig. 11. All models give very similar impact ionization coefficients as a function of the electric field and therefore, the simulated gain is almost the same. This was not the case when using the default parameterization (see Fig. 9). The Overstraeten model with the default parameterization is overestimating the gain because $\alpha_p(E)$ is too high, while the Massey and Okuto-Crowell models are underestimating the gain because $\alpha_n(E)$ is too low.

B. Temperature Dependence of the Impact Ionization

When the gain is simulated at a temperature other than 20 °C, the disagreement between the measured gain and the one simulated with the original parameters is even more significant than the one shown in Fig. 8 for 20 °C. With the new set of parameters, optimized against the full set of experimental data taken for the five LGAD types between -15 °C and 40 °C, a good agreement between simulated and measured data is found for all temperatures. For example, the results for the HPK2-S1 LGAD type are shown in Fig. 12. As shown for the electric field strength dependence in the previous section, there is not a significant difference between the three impact ionization models with optimized parameter sets in the investigated temperature range. The new $\alpha_n(T)$ and $\alpha_p(T)$ coefficients as a function of the temperature for an electric field of $3.5 \times 10^5 \text{ Vcm}^{-1}$ are shown in Fig. 13. The three original models were underestimating $\alpha_n(T)$, while $\alpha_p(T)$ was overestimated by Massey and Overstraeten, but not by Okuto-Crowell with respect to our data. Also, despite these three models using the very different formulation for the temperature dependence of the impact ionization, the $\alpha_n(T)$ and $\alpha_p(T)$ coefficients obtained after the optimization of the parameters are in good agreement. From the rising deviation of the three models toward the lowest and highest temperature investigated, differences are expected outside the temperature window studied here, indicating that any projection toward lower or higher temperature should be treated with great care.

C. Error Discussion

To understand the validity of the new parameterization, it is important to understand the sources and influence of the errors

in the method. Taking as an example the HPK2-S1 LGAD, we show how the errors in the input data can strongly modify the simulated gain and therefore give different values for the impact ionization coefficients.

- 1) A potential source of error lies in the experimental measurement of the gain. Assuming that there is no uncertainty in the reverse bias voltage and temperature, the main uncertainty arises from the already mentioned gain reduction mechanism [14]. For the HPK2-S1 LGAD, we obtain a gain of 25 at 80 V and 20 °C when the gain reduction is negligible, but if the laser intensity is increased to 10 MIPs ($\times 10$ charge density) the measured gain will drop to a value of 17. This effect will be even stronger at higher gain values. Therefore, such an error will lead to a model that will underestimate the gain.
- 2) The doping profile of the GL that is needed to generate the electric field map in the TCAD device model is also a critical input. In this regard, an error in the active boron concentration or in the position of the GL doping profile will lead to a modification in the electric field profile and therefore, will affect the parametrization of the models. For example, a decrease of 2% in the concentration of the GL or a shift of the GL position by 200 nm closer to the front electrode, will drop the simulated gain from a value of 25 (at 80 V and 20 °C) to a value of 17. Uncertainty in any of these two parameters will lead to a model that, depending on the direction of the error, underestimates or overestimates the gain.
- 3) The final boron concentration profile and position of the GL used to simulate the electric field profile, should ideally be adjusted using the measured capacitance curve of the LGADs, which can be reliably measured and simulated and thus, used to minimize the error introduced by these two parameters. However, this requires exact knowledge of the LGAD geometrical structure, including the device periphery, e.g., JTE and guard rings. A doping profile extracted from $C-V$ curves assuming a parallel plate sensor geometry with fixed area A (see Section II-A) is not sufficient in this sense.
- 4) Discretization errors in the simulations can also be a source of errors, in particular for the calculation of the gain, and should be investigated by variation of the number of nodal points. In our case, custom C++ and TCAD device simulations yielded the same gain curves giving confidence in not being impacted by this error.

If we take into account all these possible uncertainties, the error estimation in the modeling of the electric field and therefore, in the simulated gain is complicated. Thus, an approximation of the uncertainty in the new parameterization can be extracted from the dispersion in the impact ionization parameters obtained by the three different models studied. In this way, we can conclude that the error in the impact ionization parameters should be around 10% in the range of electric fields and temperatures studied. For the experimental measurement of the gain, the measured error was $\sim 5\%$.

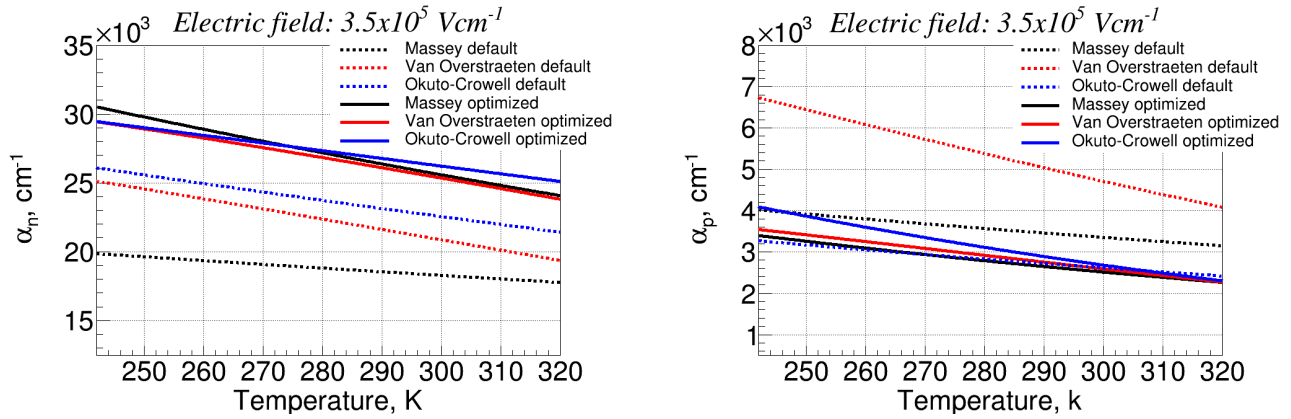


Fig. 13. New impact ionization coefficients as a function of the temperature for $E = 3.5 \times 10^5 \text{ Vcm}^{-1}$. Default values for the coefficients are also included.

V. SUMMARY

We present a new parameterization of “local” impact ionization coefficients in silicon devices. The parameterization is derived from a large set of pulsed IR-laser-based gain measurements on five different types of LGADs including devices with deep and shallow GLs. New parameters are provided for the three most commonly used models in the LGAD community: Massey, Overstraeten, and Okuto-Crowell.

The original parameterization of these models did not provide a satisfactory agreement with our experimental data motivating the presented work. TCAD device models were conceived for all LGADs based on the available knowledge about the used devices including mask files, processing information, doping profiles measured with SIMS, as well as TCT and capacitance–voltage (CV) measurements. The TCAD simulations yielded the electric field strength maps that were then used in custom-written software to optimize the parameters in the three different impact ionization coefficient models. After the parameter optimization, all three models give very similar solutions for the gain in very good agreement with the measured data. We estimate an error of $\sim 10\%$ in the parametrization obtained and its validity covers the range in temperatures from -15°C to 40°C , and a range in electric fields from 2.8×10^5 to $4.5 \times 10^5 \text{ Vcm}^{-1}$, and a maximum gain of 100 for the used LGAD devices.

ACKNOWLEDGMENT

This work has been performed in the framework of the RD50 collaboration and the CERN EP research and development program on technologies for future experiments. The authors would like to thank Salvador Hidalgo from CNM, Barcelona, Spain for the detailed information provided on the LGADs produced at CNM.

REFERENCES

- [1] G. Pellegrini et al., “Technology developments and first measurements of low gain avalanche detectors (LGAD) for high energy physics applications,” *Nucl. Instrum. Methods Phys. Res. A, Accel. Spectrom. Detect. Assoc. Equip.*, vol. 765, pp. 12–16, Nov. 2014.
- [2] H. F.-W. Sadrozinski, A. Seiden, and N. Cartiglia, “4D tracking with ultra-fast silicon detectors,” *Rep. Prog. Phys.*, vol. 81, no. 2, Dec. 2017, Art. no. 026101.
- [3] *Technical Proposal for a MIP Timing Detector in the CMS Experiment Phase 2 Upgrade*, document CERN-LHCC-2017-027, LHCC-P-009, CERN, Geneva, Switzerland, Dec. 2017.
- [4] *Technical Proposal: A High-Granularity Timing Detector for the ATLAS Phase-II Upgrade*, document CERN-LHCC-2018-023, LHCC-P-012, CERN, Geneva, Switzerland, Jun. 2018.
- [5] K. Wu, M. Zhao, T. Yang, J. G. Da Costa, Z. Liang, and X. Shi, “Design and fabrication of low gain avalanche detectors (LGAD): A TCAD simulation study,” *J. Instrum.*, vol. 15, no. 3, Mar. 2020, Art. no. C03008.
- [6] W. Maes, K. De Meyer, and R. Van Overstraeten, “Impact ionization in silicon: A review and update,” *Solid-State Electron.*, vol. 33, no. 6, pp. 705–718, Jun. 1990.
- [7] D. J. Massey, J. P. R. David, and G. J. Rees, “Temperature dependence of impact ionization in submicrometer silicon devices,” *IEEE Trans. Electron Devices*, vol. 53, no. 9, pp. 2328–2334, Sep. 2006.
- [8] R. Van Overstraeten and H. De Man, “Measurement of the ionization rates in diffused silicon p-n junctions,” *Solid-State Electron.*, vol. 13, no. 1, pp. 583–608, May 1970.
- [9] Y. Okuto and C. R. Crowell, “Threshold energy effect on avalanche breakdown voltage in semiconductor junctions,” *Solid-State Electron.*, vol. 18, pp. 161–168, Feb. 1975.
- [10] P. Agarwal, M. J. Goossens, V. Zieren, E. Aksen, and J. W. Slotboom, “Impact ionization in thin silicon diodes,” *IEEE Electron Device Lett.*, vol. 25, no. 12, pp. 807–809, Dec. 2004.
- [11] M. Mandurrino et al., “Numerical simulation of charge multiplication in Ultra-Fast Silicon Detectors (UFSD) and comparison with experimental data,” in *Proc. IEEE Nucl. Sci. Symp. Med. Imag. Conf. (NSS/MIC)*, May 2017, pp. 1–4.
- [12] T. Croci et al., “TCAD simulations of non-irradiated and irradiated low-gain avalanche diodes and comparison with measurements,” *J. Instrum.*, vol. 17, no. 1, Jan. 2022, Art. no. C01022.
- [13] T. Yang et al., “TCAD simulation and radiation damage modeling for low gain avalanche detector,” Tech. Rep., 2021. [Online]. Available: <https://doi.org/10.1016/j.nima.2022.167111>
- [14] E. Currás, M. Fernández, and M. Moll, “Gain reduction mechanism observed in low gain avalanche diodes,” *Nucl. Instrum. Methods A*, vol. 1031, May 2022, Art. no. 166530.
- [15] E. C. Rivera, “Advanced silicon sensors for future collider experiments. Sensores de silicio avanzados para futuros experimentos colisionadores,” Univ. Cantabria, Santander, Spain, Tech. Rep. CERN-THESIS-2017-212, Sep. 2017.
- [16] D. Schroder, *Semiconductor Material and Device Characterization*. Hoboken, NJ, USA: Wiley, 2015.
- [17] (Sep. 2022). *Technology Computer Aided Design (TCAD) Synopsys*. [Online]. Available: <https://www.synopsys.com/silicon/tcad.html>
- [18] R. J. McIntyre, “A new look at impact ionization—Part I: A theory of gain, noise, breakdown probability, and frequency response,” *IEEE Trans. Electron Devices*, vol. 46, no. 8, pp. 1623–1631, Aug. 1999.
- [19] A. G. Chynoweth, “Ionization rates for electrons and holes in silicon,” *Phys. Rev.*, vol. 109, no. 5, pp. 1537–1540, Mar. 1958.